BIOSYNTHESIS OF (ZnO–*ALOE VERA*) NANOCOMPOSITES AND ANTIBACTERIAL/ANTIFUNGAL STUDIES

A. AYESHAMARIAM[a*], M. KASHIF[b],V. S. VIDHYA[c],
M. G. V. SANKARACHARYULU[d],V. SWAMINATHAN[e], M. BOUOUDINA[f,g],
M. JAYACHANDRAN[h]
[a]*Department of Physics, Khadir Mohideen College, Adirampattinam 614 701, India*
[b]*Nano Biochip Research Group, Institute of Nano-Electronic Engineering (INEE), Universiti Malaysia Perlis (UniMAP), Kangar 01000, Perlis, Malaysia*
[c]*Department of Chemistry, Chendhuran College of Engineering and Technology, Pudukottai, 622 507, India*
[d]*Arignar Anna Government Arts & Science College, Karaikal , Karaikal District, 609605, India*
[e]*School of Material Science and Engineering, Nanyang Technological University, Singapore 639798, Singapore*
[f]*Nanotechnology Centre, University of Bahrain, PO Box 32038, Kingdom of Bahrain*
[g]*Department of Physics, College of Science, University of Bahrain, PO Box 32038, Kingdom of Bahrain*
[h]*Electro Chemical Material Science Division, (CSIR) Central Electro Chemical Research Institute, Karaikudi 630 003, India*

Development and analysis of disease treatments and preventive measures to avoid any dangerous outbreak of epidemic proportions are important. Modern methods of detection and treatment include tissue culture, nanotechnology, radiation, and laser technology. We report the synthesis of nanocrystalline materials by combustion methods with *Aloe vera* extract powder. ZnO + *A. vera* produces a change in its structural and optical properties. Structure, microstructure and optical characterizations of the as-prepared nanocrystalline ZnO (ZnO + *A. vera*) powders were carried out using XRD, TEM and SEM to determine their morphology. Antibacterial and antifungal tests show that ZnO nanoparticles mixed with *A. vera* are effective in inhibiting bacterial growth.

(Received July 17, 2014; Accepted September 11, 2014)

Keywords: Antimicrobials; Biodegradation; Escherichia coli; Indicators; Microbial Structure

1. Introduction

Researchers have focused on the development of efficient green chemistry methods for the synthesis of nanoparticles (NPs) on an anvil, which is also an eco-friendly method. Among these techniques, plants are the most promising candidates because of their ability to biosynthesize NPs in a large scale. Researchers have found that synthesis is shorter in effective treatment while using NPs, whereas for chemical formulations of drugs, it is time consuming. Chemical formulation also causes serious side-effects because the chemicals that are absorbed by the body are rarely excreted, which ultimately ruins the natural defense of the body.

ZnO has high electron mobility, high thermal conductivity, good transparency, wide and direct band gap (3.37 eV), and large exciton binding energy; it can also be grown easily in various

[*]Corresponding author: aismma786@gmail.com

nanostructure forms. These unique and excellent properties make ZnO suitable in various applications, such as in optoelectronics, transparent electronics and lasing and sensing applications [1].

Moreover, ZnO is preferentially in stable hexagonal wurtzite structure at room temperature, wherein each oxygen ion is surrounded by tetrahedral zinc ions alternatively stacked along the *c-axis*. Its crystallization properties are vital in crystal growth, defect generation, and etching. Investigation on the optical properties of ZnO have been conducted since the 1960s [2]. ZnO has recently elicited attention among wide bandgap materials because of its direct wide bandgap (3.37 eV) with large exciton energy (60 meV) at room temperature [3].

Alternatively, semiconducting oxides, such as SnO_2 and In_2O_3, have become important. In particular, In_2O_3 as transparent semiconductor with a direct wide-bandgap of about 3.6 eV and an indirect band gap of about 2.5 eV [4], has been widely used in solar cells, organic light-emitting diodes, batteries, and transparent thin film infrared reflectors [5], etc. It has been reported that both ZnO and In_2O_3 react at high temperatures (>1000 °C) to form a series of homologous compounds [6].

A new method reported by Maensiri et al. produces In_2O_3 NPs with particle size of 5 to 50 nm using indium acetylacetonate and *Aloe vera* extract solution [7]. This simple process using cheap precursors of *A. vera* extract provides high-yield nanosized materials with well-defined crystalline structure and good optical properties. This method can also be adopted to prepare various nanocrystalline oxides. Renugadevi and Ashwini [8] reported the biological synthesis of NPs, wherein the reducing agent can be any bio-source. Silver NPs were synthesized using *Azadirachta indica* leaf extract as a reducing agent by microwave irradiation method.

Aloe barbadensis Miller (*A. vera*) is a perennial plant of the lily (Liliaceae) or Aloeaceae family. *Aloe* has naturalized throughout the warm regions around the world. The genus *Aloe* contains over 400 different species, among which *A. barbadensis* Miller (*A. vera*), *A. aborescens*, and *A. chinensis* are the most popular. *A. barbadensis* Miller is the most biologically active [9]. Additionally, *A. vera* gel contains vitamins A (beta-carotene), C, and E, which are known antioxidants. It also has calcium, chromium, copper, selenium, magnesium, manganese, potassium, sodium, and zinc, which are essential for the proper functioning of various enzyme systems in different metabolic pathways; some of these elements are also antioxidants. *A. vera* gel provides four plant steroids: cholesterol, campesterol, β-sisosterol, and lupeol, which have anti-inflammatory action. Lupeol also has antiseptic and analgesic properties as it provides 20 out of the 22 required *amino acids* in humans and seven out of the eight essential amino acids. It also contains salicylic acid that possesses anti-inflammatory and antibacterial properties. When lignin, an inert substance, is included in topical preparation, the penetrative effect of other ingredients into the skin is enhanced. Saponins, which are soapy substances, forming about 3% of the gel and have cleansing and antiseptic properties [10]. Moreover, *A. vera* gel is a viscous, colorless, transparent, and odorless liquid with a slightly bitter taste. Generally, identity tests are established in accordance with national requirements, usually for its polysaccharide composition shown in Fig. 1.

Biological methods using plant extracts and microorganism have been proposed as alternative environment-friendly methods in the synthesis of metallic nanoparticles because chemically formulated drugs cause side-effects.

In the current study, a novel synthesis for In_2O_3 and ZnO NPs with particle sizes on the range 10 to 30 nm using indium nitrate and zinc nitrate solutions, is reported. NPs are formed by combustion of the dried precursors in a furnace at 300 °C for 3 min. This method utilizes *A. vera* extract from the solution as a solvent instead of organic solvents. Pure extract powders are prepared by using the method in a previous report [11]. This method is inexpensive, nontoxic, and uses environmentally safe precursors. This cost-efficient source of *A. vera* extract provides high-yield nanosized materials with good crystalline structure and good optical properties. The proposed method can also be used to prepare nanocrystalline oxides of other materials.

The antibacterial activities of synthesized NPs (ZnO and In_2O_3) have also been studied. Antibacterial activities of ZnO, In_2O_3, *A. vera* + ZnO, *A. vera*+ In_2O_3, and ZnO + In_2O_3 + *A. vera* NPs have been assessed against the microorganisms *Staphylococcus aureus*, *Escherichia coli*,

Salmonella typhi, *Pseudomonas aeruginosa*, and *Streptococcus pyogenes*, as well as antifungal microorganism *Aspergillus niger*, by disc diffusion method.

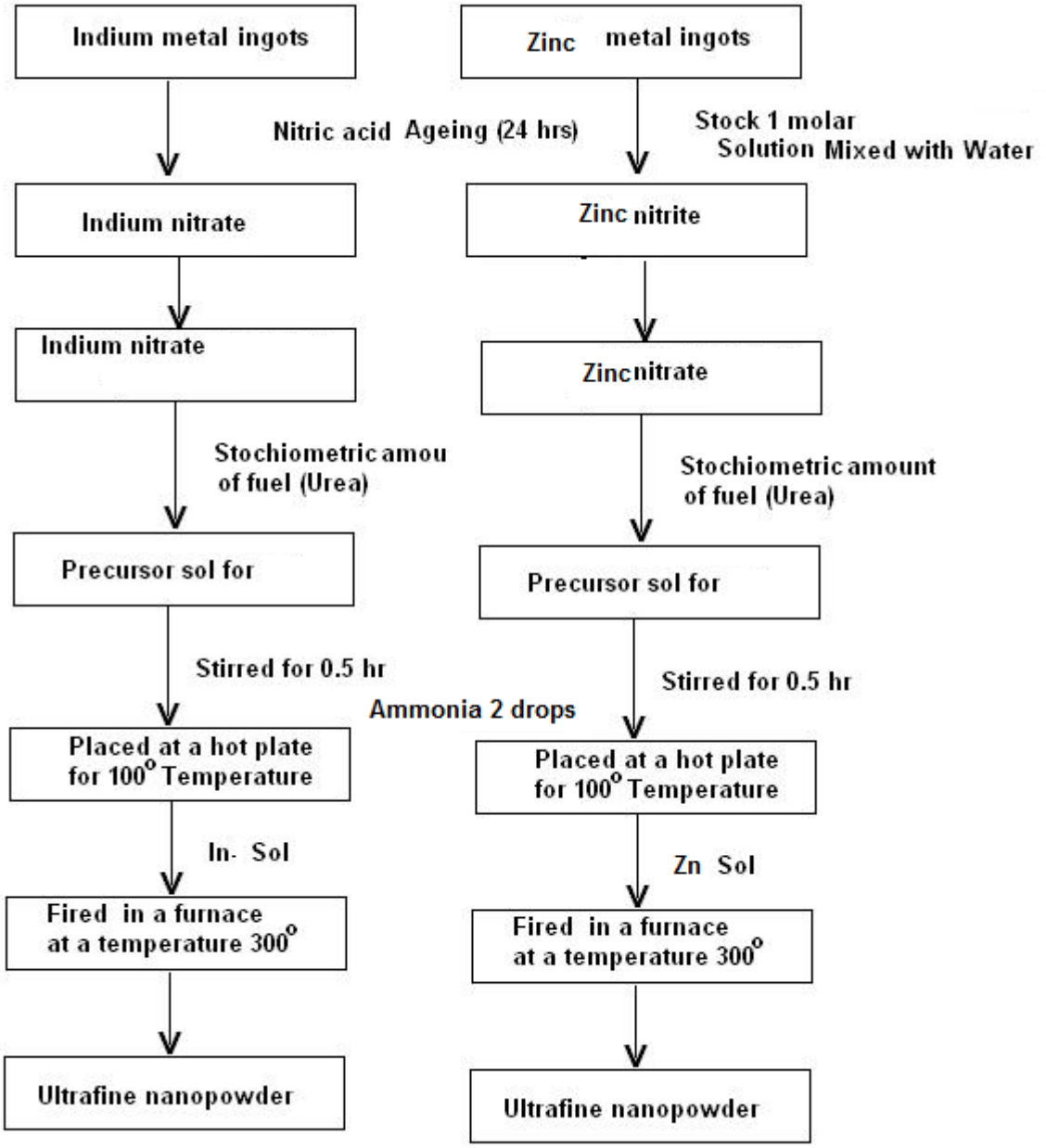

Fig, 1. Schematic preparation route of In_2O_3 and ZnO nanoparticles

2. Experimental Part

2.1 Samples Preparation

A solution of (0.5 M) of $In(NO_3)_3 \cdot 3H_2O$ and $Zn(NO_3)_2 \cdot 6H_2O$ dissolved in water was prepared. After that, the solution attained equilibrium, ammonia solution was added drop-wise into the mixed precursor solution until it reached pH 6. The mixture was then diluted with water and magnetically stirred for 1 hour. Oxygen-balanced amount of fuel urea was added to the mixture until a gel of indium oxide and zinc oxide appeared. The mixture was stirred for another 1 hour at ambient temperature. The pH of the solution was maintained in the range of 5 to 6. The solution

was stirred again for 1 hour to ensure that precipitation was complete. The solution was then placed in a hot plate at 100 ºC until it decomposed into a gel-like foam structure. The product was placed in a furnace and fired at 300°C to obtain the dried nanopowder.

2.2 Characterization Techniques

X-ray diffraction (XRD) was performed using a Philips X-ray diffractometer with Cu-Kα radiation (λ = 0.15406 nm). The particle size and morphology of the calcined powders were characterized by transmission electron microscopy (TEM, Hitachi H8100 200 kV). Scanning electron microscopy (SEM) analysis was conducted using Hitachi S-4500 SEM machine. Optical absorption spectra were measured from 200 to 800 nm using a Shimadzu UV-3101PC UV–VIS–NIR scanning spectrometer. Photoluminescence (PL) measurement was carried out on a luminescence spectrometer Perkin–Elmer LS-55B using a xenon lamp as the excitation source at room temperature (the samples were dispersed in dichloromethane) with an excitation wavelength of 250 nm.

2.3 Extraction of antimicrobial ingredients from A. vera leaves

The powder was obtained from *A. vera* leaf extract solution using a freeze dryer by rapidly freezing the peel and then eliminating the water by sublimation. The phosphate buffered saline (PBS) used in this study had a final concentration of 137 mM of sodium chloride, 2.7 mM of potassium chloride, 4.3 mM of sodium phosphate (dibasic), and 1.4 mM of potassium phosphate (monobasic). Distilled water (DW) was used for the extraction, considering the economic use for large-scale industrial applications [9]. Exactly 50 g of the material was added to 500 ml of DW, which was shaken at a speed of 250 rpm for 8 hours at room temperature. The solution was then centrifuged at 3000 rpm for 50 min. The supernatant was filtered through No. 5A filter paper, and the filtered solution was again freeze-dried. A total of 1 g of the dried powder was dissolved in 1.5 ml of DW to form a saturated solution.

2.4 Preparation of Nanocomposites

To obtain *A. vera* leaf extract with oxides nanocomposites materials, 1 g of the dried powders (ZnO and In_2O_3) were dissolved in 1.5 ml of DW, separately. Equal ratio of these two solutions were well stirred and dried using a hot plate at 40ºC (natural temperature of *A. vera* leaf extract). A total of 1 g of In_2O_3 and 1 g of ZnO powder of the same ratio of *A. vera* dried powder were separately dissolved in two 1.5 ml of DW to obtain the nanocomposite dried powder.

2.5 Evaluation of antibacterial and antifungal activities

The supernatant was collected and stored in a refrigerator at 4°C. Different concentrations of *A. vera* extracts were subjected to antimicrobial studies. Five bacterial cultures were maintained in nutrient agar medium at room temperature and sub-cultured into newly prepared nutrient agar slants every two weeks.

2.5.1 Well Diffusion Method

Antibacterial and antifungal activities of the plant extract were tested using well diffusion method [12]. The prepared culture plates were inoculated with different strains of bacteria and fungi using streak plate method. Wells were made on the agar surface with a 5 mm cork borer. The extracts were poured into the well using a sterile syringe. The plates were incubated at 37±2°C for 48 hours for fungal activity, and for 24 hours for bacterial activity. The plates were observed for the zone formation around the wells.

The extracts of *A. vera*, nanocomposites oxides ZnO, In_2O_3, *A. vera* + ZnO, *A. vera* + In_2O_3 and *A. vera* + ZnO + In_2O_3 were used throughout the study. The extracts were dissolved in

sterile distilled water to form dilutions with 5, 10, and 25 µg of the extracts. Each concentration of the drug was tested against different bacterial pathogens for antibacterial activity using well diffusion assay [13]. One species each of Gram-positive bacteria and Gram-negative bacteria (*P. aeruginosa* MTCC-3542) were used for the antibacterial assays.

The zone of inhibition was calculated by measuring the diameter of the inhibition zone around the well (in mm), including the well diameter. The readings were taken in three different fixed directions in all three replicates, and the average values are tabulated in Table 2.

Table 1. XRD results of ZnO, Alovera + ZnO, In_2O_3, Alovera + In_2O_3, and Alovera + ZnO + In_2O_3

Sample	Grain size(nm)	Strain= $\beta \cos\theta / 4$	Dislocation density $\frac{1}{D^2}$ lines/m^2	Lattice parameter	Volume (m^3)
ZnO	27.33	0.0053	1.339×10^{15}	a = 3.248 c = 5.192 c/a = 1.598	$a^2{}_{C\ Sin\theta}$ = 47.104
Alovera + Zin oxide	69.02	0.01218	2.099×10^{14}	a = 3.112 c = 5.001 c/a = 1.607	$a^2{}_{C\ Sin\theta}$ = 41.94
Indium oxide	11.010	0.00329	0.8249×10^{16}	10.22	a^3 = 1067.09
Alovera Indium oxide + Zinc oxide	47.32	0.02145	4.527×10^{14}	a = 2.963 c = 5.023 c/a = 1.695	$a^2{}_{C\ Sin\theta}$ = 38.189

Table 2. Antifungal activities with different microorganism of different zone of inhibition (mm)

S. No	Bacteria	Zone of Inhibition (mm)																	
		Sample A (In_2O_3 +Alovera)			Sample B (ZnO +Alovera)			Sample D (ZnO +In_2O_3 +Alovera)			Sample E (In_2O_3)			Sample F ZnO			Sample G(Alovera)		
		5 mg	10 mg	25 mg	5 mg	10mg	25mg	5 mg	10 mg	25 mg	5 mg	10 mg	25 mg	5 mg	10 mg	25 mg	5 mg	10 mg	25 mg
1	*Staphylococcus aureus*	7	10	19	7	12	20	8	10	22	8	12	14	14	20	24	15	17	22
2	*Escherichia coli*	-	-	-	-	-	-	7	16	20	0	16	18	-	-	-	-	-	-
3	*Salmonella typhi*	-	-	-	14	16	20	7	9	10	-	-	-	-	-	-	-	-	-
4	*Pseudomonas aeruginosa*	12	14	19	10	12	24	9	12	18	6	12	20	12	15	17	18	21	24
5	*Streptococcus pyogenes*	-	-	-	-	-	-	10	12	14	-	-	-	-	-	-	17	18	21

The methanolic and aqueous extracts of 100, 200, and 500 mg of *A. vera* extract powder, *A. vera* extract with ZnO, *A. vera* extract with In_2O_3, and *A. vera* powder with ZnO and In_2O_3 were used for the antifungal activities.

(a) Bacterial Media (Muller–Hindon medium)

A total of 36 g of Muller–Hindon medium (Hi-medium) was mixed with distilled water and then sterilized in an autoclave at 15 liquid bowl pound (lbp) pressure for 15 min. The sterilized media were then poured onto Petri dishes. The solidified plates were pored with 5 mm diameter cork borer. The plates with wells were used for the antibacterial studies. The solidified plates were pored with 6 mm diameter cork borer

(b) Fungal Media (Sabouraud agar medium)

A total of 10 g of peptone was mixed with distilled water, and 40 g of dextrose was mixed with the peptone infusion. Then, 20 g of agar was added as a solidifying agent. These constituents were mixed and autoclaved. The solidified plates were pored with 5 mm diameter cork borer.

(c) Bacterial Strains

The bacterial and fungal pathogenic strains were obtained from the Microbial Type Culture Collection (MTCC), the Institute of Microbial Technology, Sector 39-4 Chandigarh, India. Bacterial strains were *S. aureus* (MTCC-737), *S. pyogenes* (MTCC-1923), *P. aeruginosa* (MTCC-3542), *E. coli* (1576), and *S. typhi* and were maintained at 4 ºC on nutrient agar.

(d) Fungal Strains

Fungal strains were *A. niger* (MTCC-1344), *A. flavus* (MTCC-1973), *A. fumigatous* (MTCC-2132), *Rhizopusindicus*, and *Mucorindicus* (MTCC-918).

3. Results and Discussion

3.1 Structural Characterization

XRD pattern of ZnO powder confirms the presence of a high-quality hexagonal wurtzite crystalline structure (Fig. 2a), in agreement with JCPDS, Card No. 36-1451 [4], with lattice parameters are a = 3.249 Å and c = 5.206 Å and mean crystallite size as calculated using sheerer's equation around 27 nm.

In_2O_3 crystallizes within the C-M_2O_3 (bixbyite) structure in agreement with JCPDS Card No. 6-416) [4], with lattice parameter a = 10.117 Å and mean crystallite size as calculated using sheerer's equation around 11 nm (Fig. 2). The observed reflections are assigned to the (222) and (400) planes, indicating a preferential growth of crystallites along the (222) plane. Effective surface area for ZnO and In_2O_3 decreases because of the incorporation of *A. vera*, thereby decreasing the optical activities. When *A. vera* is doped with ZnO, In_2O_3 optical properties show the lowest adsorption of extract, and their initial value of saturation is very low compared with that of other samples. For the present case, the observed large crystal sizes confirm that no dependency between the energy gap and the crystal size would be expected

Dispersion stability decreased by the incorporation of *A. vera* would also result in lesser absorption of *A. vera* extract on the surface, and may be the reason for low degradation. Therefore, higher dopant concentration results in less effective surface absorption of A.vera, which is necessary for reactions and lower degradation of A.vera.

Uniform particle size distribution is important for nanocrystalline systems. However, the addition of *A. vera* to oxide materials (In_2O_3 and ZnO) to form nanocomposites results in an increase in particle size. If segregation of additives occurs, both In_2O_3 and ZnO particles are agglomerated with *A. vera* extract powder, thereby decreasing the crystallinity of the powder. Given that the XRD pattern of In_2O_3 + *A. vera* looks typical of amorphous phase, thereby it was not possible to calculate the full width at half maximum (FWHM), which helps to estimate the crystallite size. For ZnO + *A. vera*, only one peak is observed with minimum relative intensity giving a mean crystallite size of 69 nm. For ZnO + In_2O_3 + *A. vera* composite, the estimated crystallite size is about 47 nm, and the XRD pattern shows a crystallized powder with no uniformity (Table 1).

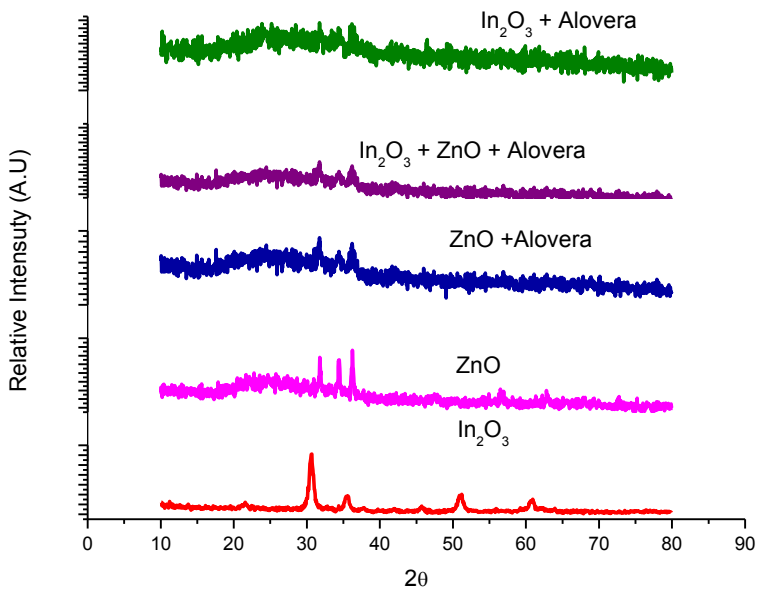

Fig. 2. XRD results of all the samples except alovera powder

If the crystallite size of pure ZnO and In_2O_3 becomes smaller, the surface area remarkably increases, making the surface properties important and determinant of the properties of the as-prepared nanocomposites. Given that, when the nanomaterials are mixed with *A. vera* extract, diffusion and hygroscopicity of the particles may occur, resulting in a possible a decrease in the surface area, which reduces the surface energy.

3.2 TEM Analysis

The high-resolution lattice images suggest that the nanopowders are crystalline and that the distance between two lattice planes is similar in ZnO and In_2O_3 phases, which corresponds to the d-spacing of (001) crystal planes of wurtzite ZnO. Figs. 3a and 3b show TEM images of ZnO+ A.vera and In_2O_3 + A.vera composites. Significant changes are observed in the particle morphology because of the addition of *A. vera* in the ZnO + In_2O_3 + *A. vera* composite (Fig. 3a). The TEM image of ZnO + In_2O_3 + *A. vera* nanocomposite confirms the general morphologies seen in SEM observation (Section 3.3). Individual belt-like nanostructures frequently exhibit a doped-crystal nature with obvious contours. The ends of these nanobelts exhibit some peculiar morphologies, such as irregular-triangle heads.

Such peculiar structures are further analyzed in detail using analytical TEM. Fig. 3c shows the bright-field TEM images of a ZnO + In_2O_3 + *A. vera* with irregular-triangle head. The diagram for the lattice structure of diffraction pattern is also shown in Fig. 3d. The diameter of the belt is about 60 nm and its length is up to 50 mm (shown in this figure). The bright–dark stripes in the body of the nanostructures (indicated by the arrows) are mostly ZnO planes (110) and (001) planes. For In_2O_3, a multiple crystalline nature of the nanocomposites is observed.

A significant change is observed in the morphology of ZnO + In_2O_3+ *A. vera* nanocomposite, which has more oxygen vacancies with appropriate ratios reflected in the bandgap of UV–Vis studies (Section 3.3). ZnO and In_2O_3 combined with *A. vera* powder show microstructures (TEM and SEM) that are prone to quick agglomeration (80 nm clusters). No further annealing is carried out to avoid such agglomeration. The TEM image of In_2O_3 + *A. vera* and ZnO + *A. vera* nanoparticles exhibits larger sizes and shapes from 80 nm to 100 nm. For ZnO + In_2O_3 + *A. vera* particles, the size decreases up to about 50 nm. Therefore, ZnO + In_2O_3 + *A. vera* nanocomposite produces very small particles with a predominant ZnO (110) reflection.

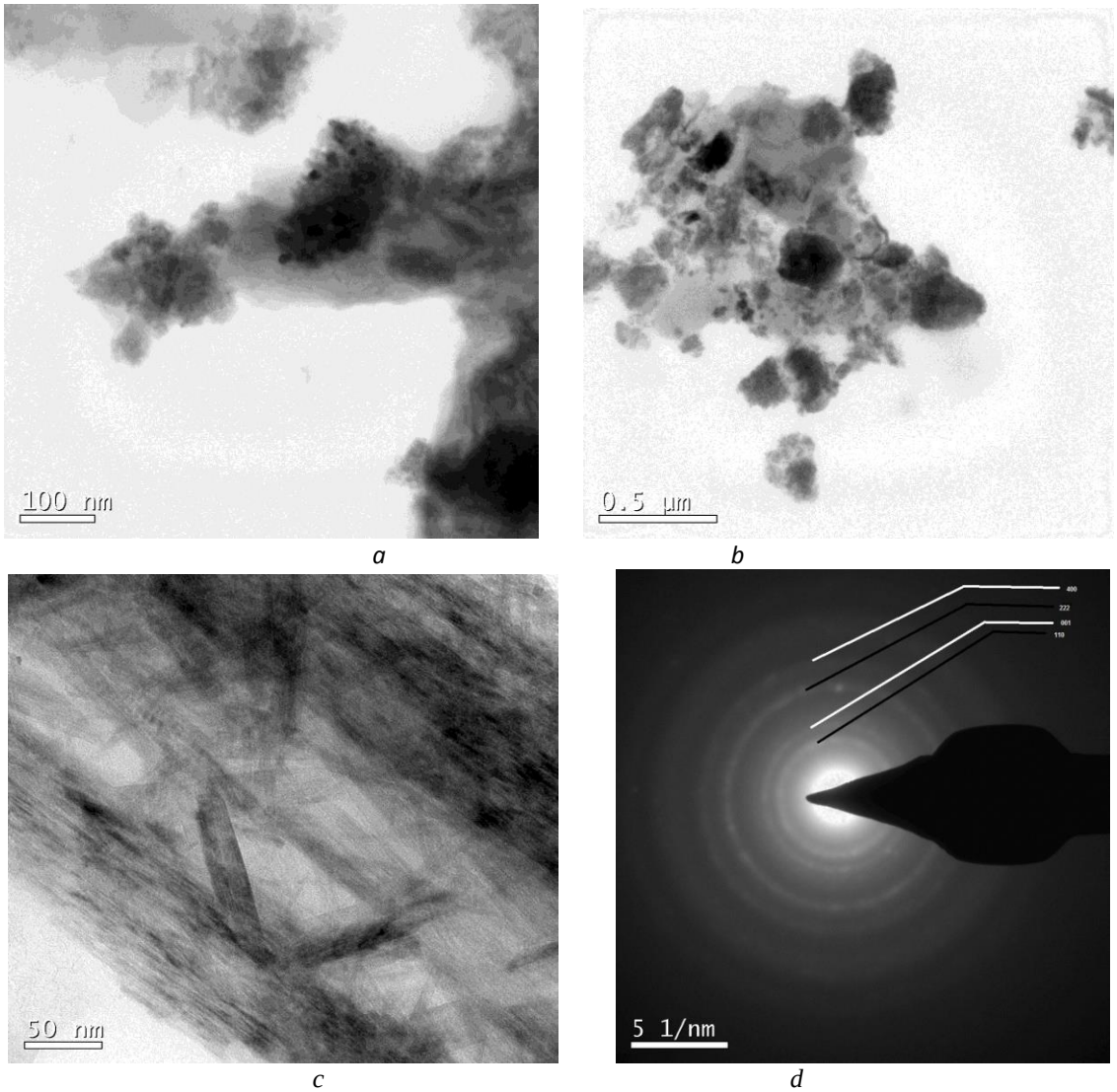

a *b* *c* *d*

Fig. 3(a). TEM image of (ZnO + Alovera), (b). TEM image of (In_2O_3 + Alovera), (c). TEM image of (ZnO + In_2O_3 + Alovera), (d). SAED pattern of (ZnO + In_2O_3 + Alovera)

3.3 SEM Analysis

SEM images of In_2O_3, ZnO, ZnO + *A. vera*, In_2O_3 + *A. vera*, and ZnO + In_2O_3 + *A. vera* nanopowders, are interconnected, but the third nanocomposite has a three-dimensional structure shown in Fig. 4 with good mechanical strength, as observed in TEM. The microstructural changes during the process with *A. vera* lead to a decrease in pore size and diameter, resulting in an agglomeration of the particles. The microstructural changes are accompanied by the associated internal stresses in the membrane of nanocomposites. Adding *A. vera* to ZnO and In_2O_3 can lead to local shifts in the interconnected grains, thereby reducing internal stresses. This observation results in a decrease in the band gap of the nanocomposites (see section 3.4). SEM morphology of the oxide product strongly depends on the precursor system, and its composites (ZnO + In_2O_3) exhibit good incorporation of *A. vera* extracts, wherein a well-defined and easily accessible crystal surface is observed. However, the SEM images reveal a surface layer with a different crystallinity that may explain the high content of ZnO + In_2O_3 at the A.*vera* surface. As no other crystalline structure different from ZnO was found on the XRD data, A.*vera* must be amorphous and with a high In content, probably In_2O_3, being this effect more important for the less its formation may be related to the slow growing rate at these nanocomposites.

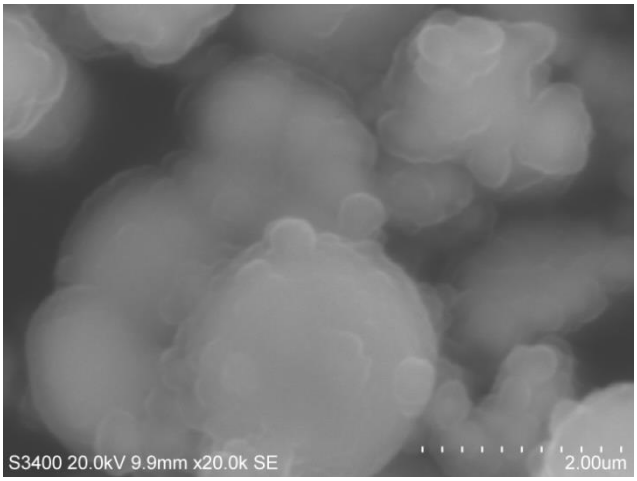

Fig. 4. SEM photograph of (ZnO + In_2O_3 + Alovera)

3.4 Optical Studies

Semiconducting nanoparticles exhibit a change in their electronic properties relative to the bulk counterpart. As the size of the particles becomes smaller, the band gap becomes larger. Likewise, as *A. vera* extracts are mixed with ZnO, In_2O_3 and ZnO + In_2O_3 bulk bandgap energies shift to the red region, *i.e.*, the particle size increases resulting in the decrease of bandgap value, but the third nanocomposite enhances the results of pure ZnO and In_2O_3 (NOT CLEAR).

ZnO, In_2O_3, ZnO + *A. vera*, and In_2O_3 + *A. vera* composites rapidly turn into dark green whereas ZnO + In_2O_3 + *A. vera* powder turns into black. The absorption band in the NIR region is shown in Fig.5a.

Optical absorption and emission spectra of ZnO + *A. vera*, In_2O_3 + *A. vera*, and ZnO + In_2O_3 + *A. vera* show that the related absorption or emission peak shifts toward the red region as the particle size increases (Fig. 5a). However, even the most highly colored products have low optical absorption in the visible region of the spectrum; thus, in this case, they can also be considered transparent conductors.

UV–Vis spectroscopy showed that although ZnO and In_2O_3 have UV emissions which can be attributed to excitonic transitions, for ZnO + *A. vera*, In_2O_3 + *A. vera*, and ZnO + In_2O_3 + *A. vera*, UV emissions could also be due to deep-level defects, which are associated with oxygen deficit (vacancies) and interstitial Zn ions (structural defect). Therefore, the slow growth rate (lower potential deposition) would result in a stronger effect in ZnO compound. Appropriate choice of experimental parameters is crucial to suppress or enhance the defect-related emission of ZnO. This finding indicates that surface states are very important to the optical properties of nanoparticles. The peaks at 486 and 520 nm may be due to Zn vacancy-related defects [14].

Fig. 5b shows the reflectance spectra of ZnO, In_2O_3, ZnO + *A. vera*, In_2O_3+ *A. vera*, and ZnO + In_2O_3 + *A. vera* nanocomposites. Fig. 5b shows that with the addition of *A. vera* concentration in equal ratio to ZnO, In_2O_3, ZnO + *A. vera*, In_2O_3 + *A. vera*, and ZnO + In_2O_3 + *A. vera*, the diffuse reflectance increases is 89% (ZnO), 60% (In_2O_3), 45% (ZnO + *A. vera*), 40% (In_2O_3 + *A. vera*), and 77% (ZnO + In_2O_3 + *A. vera*). These changes are may be attributed to the increase in surface states of Zn and In ions and the decrease in surface defects in the other first three compounds (confirmed by PL study). A broad reflectance peak from 530 nm to 600 nm of the *A. vera*-doped compounds corresponds to the dark green to the reddish portion of the visible region [15].

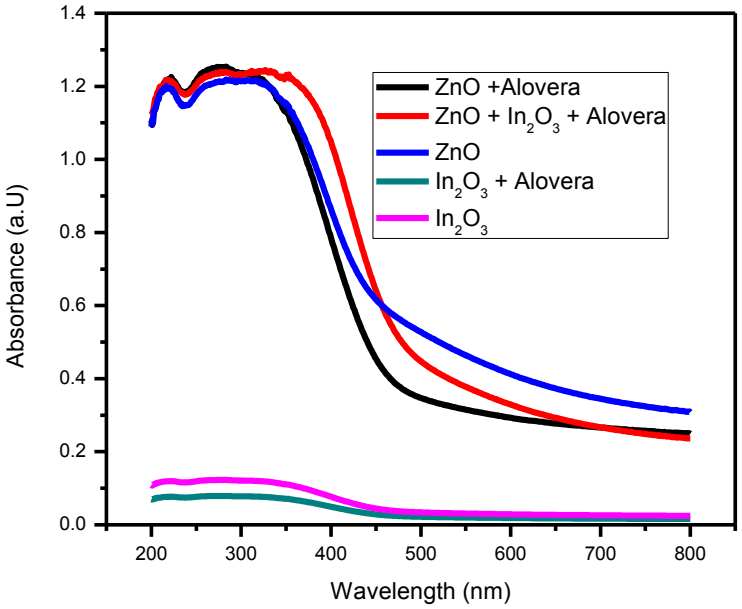

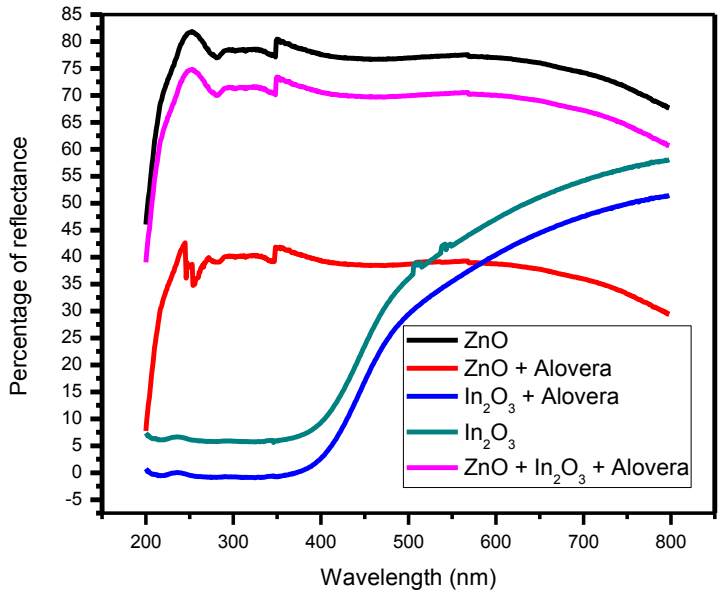

Fig. 5a. Absorption spectra of all samples except Alovera powder, b. Transmission spectra of all samples except Alovera powder

The UV–Vis absorption spectra of all the samples (Fig. 5a) exhibit strong absorption below 350 nm, with a well-defined absorbance peak at around 300 nm. The direct bandgap energy (E_g) of the nanocomposites is determined by fitting the absorption data to the direct transition equation:

$$\alpha h\upsilon = \mathrm{E}\,(h\upsilon - E_g)^{1/2} \qquad (1)$$

where α is the optical absorption coefficient, $h\nu$ is the photon energy, E_g is the direct band gap, and E is a constant [16]. Plotting $(\alpha h\nu)^2$ as a function of photon energy and extrapolating the linear portion of the curve to the absorption equal to zero (Fig. 6) gives the values of the direct band gap

(E_g): 3.76 eV for In_2O_3, 2.411 eV for In_2O_3 + *A. vera*, 3.544 eV for ZnO, 3.352 eV for ZnO + *A. vera*, and 3.476 eV for ZnO + In_2O_3 + *A. vera*.

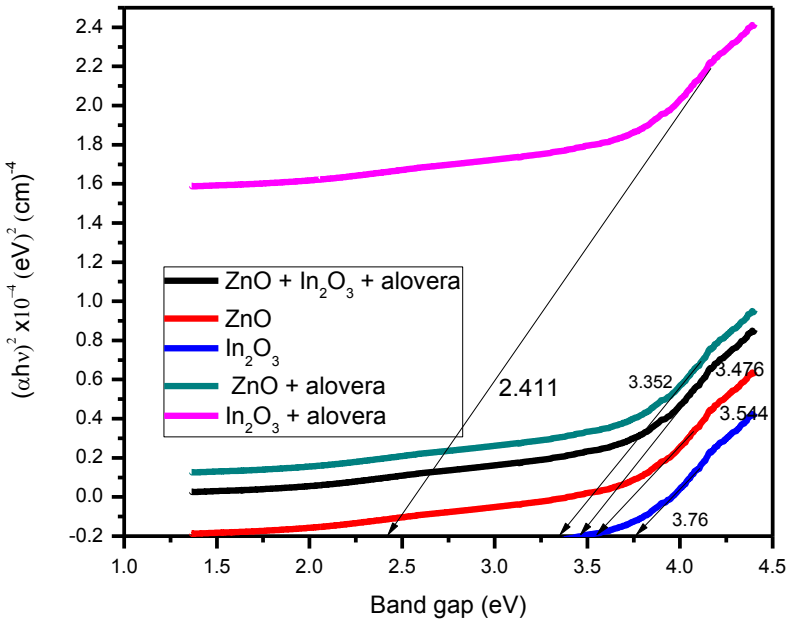

Fig. 6. Band gap values of all samples except Alovera powder

UV–Vis spectroscopy was used to characterize the optical absorption properties. UV–Vis spectra were recorded in the diffuse reflectance mode (R) using $BaSO_4$ as reference. Spectra were recorded in air at room temperature, and the data transformed through a Kubelka–Munk function relating the reflectance of the sample (Rα) to sample concentration; mathematically, $F(R) = (1-R_\infty)^2/2R_\infty$ [17].

The PL spectra of ZnO, In_2O_3, ZnO + *A. vera*, In_2O_3 + *A. vera*, and ZnO + In_2O_3 + *A. vera* at room temperature are shown in Figs. 7 and 8. Two main bands are observed: a UV emission band and a broad emission. The UV emission band is commonly attributed to the transition in the near band-edge of ZnO + In_2O_3, particularly for the nanocomposites with *A. vera* [18]. The broad emission band in the visible region (300 nm to 1200 nm) is attributed to deep-level effects in ZnO. Nanocomposites with *A. vera* are predominant and exhibit good absorbance, and thus, good optical properties. It is observed a clear influence of the shape of the particles and *A. vera* with the oxides, and nanocomposite ligands are present on the luminescence properties in the visible domain. Two additional emissions at 423 and 504 nm (Fig. 7) are associated with the presence of surface defects over the nanoparticles. The first emission corresponds to the known yellow emission, whereas the second emission appears with the presence of *A. vera*, for pure oxides, and when composite ligands are present.

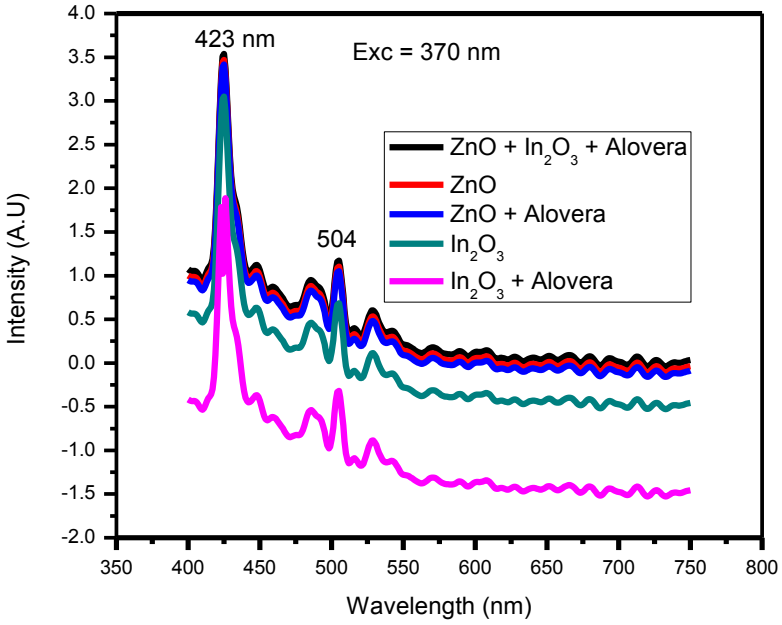

Fig. 7. Emission peak of all samples except Alovera powder

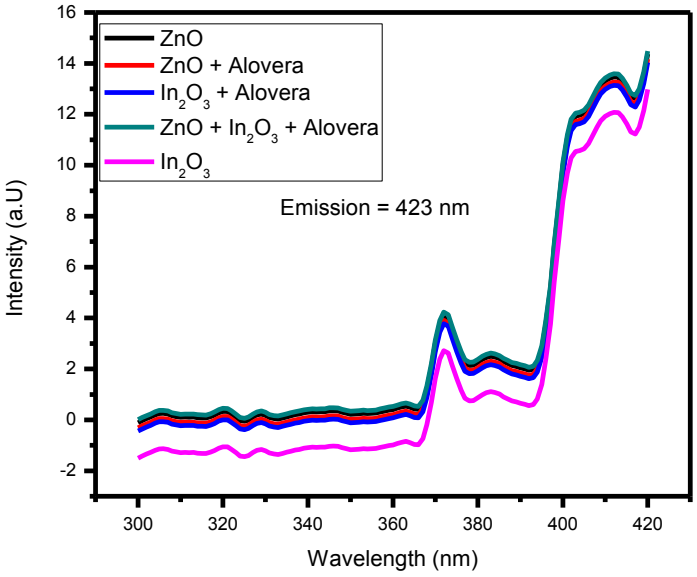

Fig. 8. Excitation peak of all sample except Alovera powder

3.5 Antibacterial and Antifungal Activities

NPs that are produced by plants are more stable, and the rate of synthesis is faster than in the case of microorganisms. NPs of ZnO and In_2O_3, as well as composites of ZnO + *A. vera*, In_2O_3 + *A. vera*, and ZnO + In_2O_3 + *A. vera*, vary in shape and size. The objectives of using *A. vera* extracts and semiconducting NPs by biosynthesis are of interest to investigate the mechanisms of uptake and bioreduction of atoms and to understand the possible mechanisms and activities with five different bacteria and one fungus.

The antibacterial activity was monitored using agar–well diffusion and agar–disc diffusion method. The activity was determined by noting the zones of inhibition around the wells or discs [19]. Antibacterial activity of *A. vera extracts* was checked against five isolates (Table 2). The percentage of Gram-positive isolates, namely, *S. aureus*, *E. coli*, *S. typhi*, and *S. pyogenes*, and the percentage of Gram-negative isolate *P. aeruginosa*, are given. *A. vera* has gained increasing antimicrobial and antifungal activities as an individual, and enriches these activities when mixed with ZnO and In_2O_3 [20].

The inhibitory effects of pure extracts of *A. vera* powder are illustrated in Table 2. The activity-dependent and comparable results are shown in Table 2. Agar diffusion tests suggest good correlation with other antimicrobial susceptibility tests. Natural extracts of *A. vera* mixed with ZnO and In_2O_3, always show better performance than their original powders. No preservatives are added in the former extracts and its composites thus avoiding biased results.

Well diffusion method was used for the assessment of antibacterial activity. Antimicrobial activities of ZnO NPs against *P. aeruginosa* and *Staphylococcus* are shown in terms of inhibition zone (mm) size in Table 2.

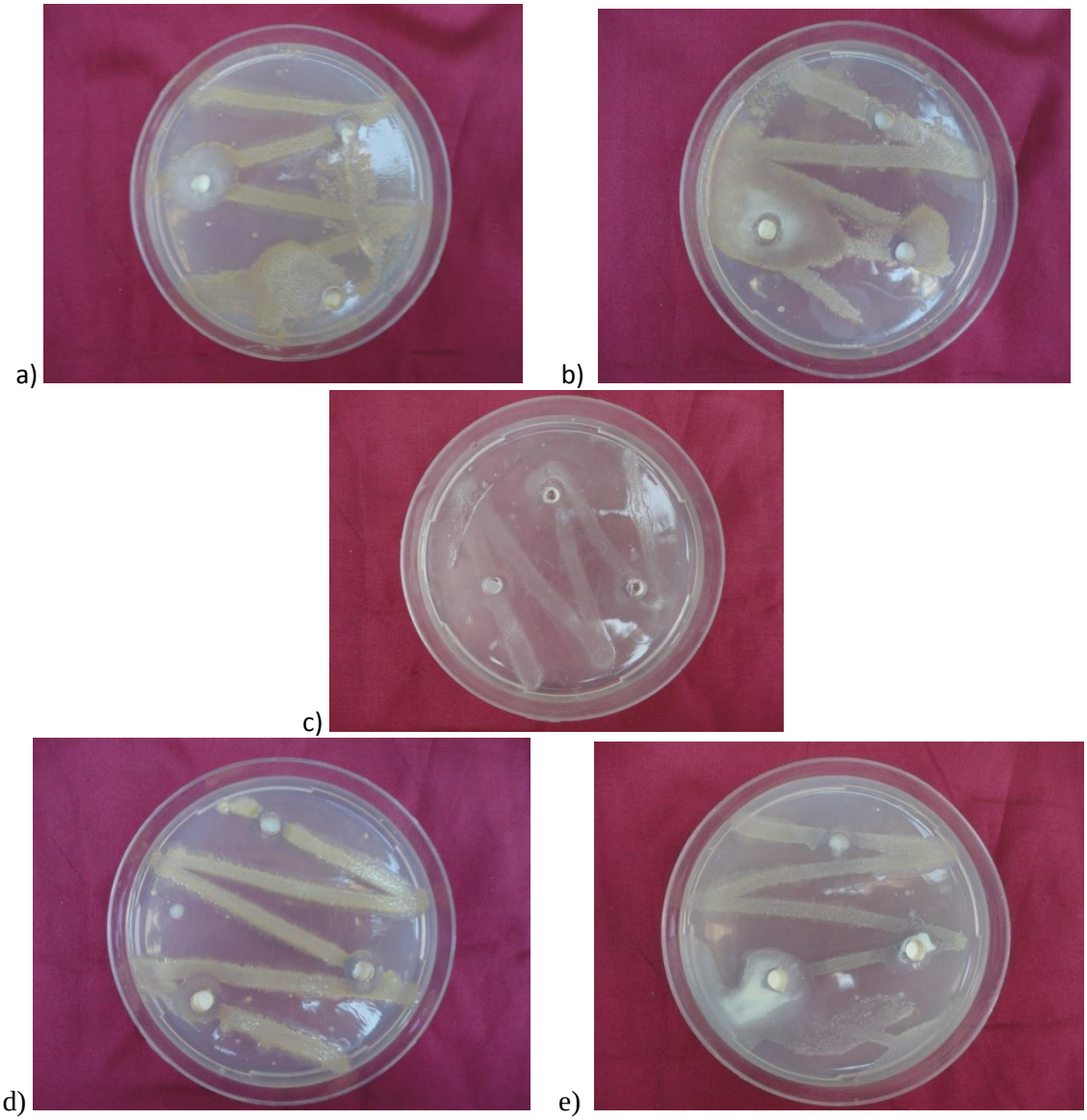

Fig. 9(a). Pseudomonas aeruginosa micro organism with (ZnO + In_2O_3 + Alovera), (b). Staphylococcus aureus micro organism with (ZnO + In_2O_3 + Alovera), (c). Salmonella typhi micro organism with (ZnO + In_2O_3 + Alovera), (d). Escherichia coli micro organism with (ZnO + In_2O_3 + Alovera), (e). Streptococcus pyogenes micro organism with (ZnO + In_2O_3 + Alovera)

Antimicrobial activities of *A. vera* + ZnO NPs against *S. typhi*, *P. aeruginosa*, *and S. aureus.* Antimicrobial activities of In_2O_3 NPs against *Staphylococcus*, *P. aeruginosa*, and *E. coli* are shown in terms of inhibition zone (mm). Antimicrobial activities of *A. vera* + In_2O_3 NPs against *S. aureus*, *P. aeruginosa*, and *E. coli*. Antimicrobial activities of ZnO + In_2O_3 + *A. vera* NPs against *P. aeruginosa*, *S. aureus*, *S. typhi*, *E. coli*, and *S. pyogenes* are shown in terms of inhibition zone (mm) size in Fig. 9(a)–(e). Antifungal activities on microorganism *A. niger* of ZnO + *A. vera*, and ZnO + In_2O_3 + *A. vera* are shown in Figs. 10(a) and 10(b). This study revealed that the tested *A. vera* plant extract have potential antibacterial activity against *S. aureus* and *P. aeruginosa*. The extracts with ZnO + In_2O_3+ *A. vera* showed the highest inhibitory activity against the tested bacteria.

a) b)

Fig. 10(a). Antifungal activities of micro organism Aspergillus niger of (ZnO + Alovera) (b). Antifungal activities of micro organism Aspergillus niger of (ZnO + In_2O_3 + Alovera)

The fungi tested in the ZnO + *A. vera* and ZnO + In_2O_3 + *A. vera* study have limited susceptibility to *A. vera* gel and extracted fractions (Figs. 10(a) and 10(b)). *A. niger* growth is inhibited by the extract. This result is important because *A. niger* is resistant to both oxide NPs with *A. vera* extracts. This study has established the susceptibilities of a broad range of bacteria to fractions isolated from *A. vera* leaf extracts with oxide NPs of ZnO, In_2O_3, and ZnO + In_2O_3. Gram-negative bacilli were found to be particularly susceptible to *A. vera* extracts, ZnO, In_2O_3, and ZnO + In_2O_3 nanocomposites. Among the bacterial classes tested, only the Gram-positive bacteria are resistant to the *A. vera* components [21, 22].

The antibacterial and antifungal activities to five different microorganisms of the samples with *A. vera* extracts may be due to the binding to the oxide NPs of ZnO, In_2O_3, and their nanocomposites, which formed novel structural, microstructural and optical properties.

4. Conclusion

Although the size of the synthesized ZnO and In_2O_3 nanopowder is smaller than the nanocomposite size, both absorption spectra and emission show a distinct red shift with the increase in size. However, the antibacterial and antifungal activities are stronger for the nanocomposites with *A. vera*. Given that ZnO + In_2O_3 + *A. vera* are nanosized, the weakly confined quantum effects agree with other reports. Therefore, the nanocomposites incorporated with *A. vera* have good absorption capacity, crystallinity, better transmission, and enriched antibacterial and antifungal activities. ZnO, In_2O_3, ZnO + *A. vera*, In_2O_3 + *A. vera*, and ZnO + In_2O_3 + *A. vera* NPs have strong antibacterial activity against *P. aeruginosa*, and the activity is increased as the concentration of ZnO NPs is increased. The unique characteristics of NPs largely increase the surface area of ZnO or enhance the affinity, so ZnO NPs exhibit stronger antibacterial activity than In_2O_3.

References

[1] S. B. Ogale, Thin films and Heterostructures for Oxide Electronics (New York:Springer), **97**, 034106 (2005),.

[2] J. K. Kim, J. L. Lee, J. W. Lee, H. E. Shin, Y. J. Park, T. Kim,. Appl. Phys. Lett. **73**, 2953 (1998).

[3] M. Kashif, M.E.Ali, Syed M.UsmanAli, U.Hashima et al., Ceramics International **139**, 6461 (2013).

[4] A. Ayeshamariam, M.Bououdina, C.Sanjeeviraja, Materials Science in Semiconductor Processing **16**, 686 (2013)–695

[5] D. Zhang, C. Li, S. Han, X. Liu, T. Tang, W. Jin, C. Zhou,..Appl. Phys. A **77,** 163 (2003).

[6] V. H. Kasper, et al.. Anorg. Allg. Chem. **349**, 113 (1967).

[7] A. Ayeshamariam, K.Tajun Meera Begam, M. Jayachandran, G. Praveen Kumar, M Bououdina, International Journal of Bioassays, ISSN: 2278-778X

[8] S. Maensiri, P. Laokul, J. Klinkaewnarong, S. Phokha, V. Promarak, S. Seraphin, J. Optoelectron. Adv. Mater. **10**(3), 161 (2008).

[9] K. Renugadevi, R.VenusAswini, Asian Journal of Pharmaceutical and clinical research, **5**, 4 (2012).

[10] S .Choi, et al, British J. of Dermatol. **145**(4), 535 (2001).

[11] A. Surjushe, et al, Aloevera: a short review. Indian J. Dermatol.**53**(4), 163 (2008).

[12] M. Grieve, et al., A Modern Herbal.Jonathan Cape, London.**12**, 26 (1975),

[13] R.K.Waihenya, M.M.Mtambo, G. Nkwengulila, U.M.Minga, et al. J. Ethnopharmacol. **79**, 317 (2002).

[14] Z. Jindal, N. K.Verma, J. Mater. Sci. **43**, 6539 (2008).

[15] E. Ziegler, A. Heinrich, H. Oppermann, G. Stover, Phys. Status Solidi A, **66**, 635 (1981).

[16] Asma Bashir, BushraSaeed, Talat .Y. Mujahid, NayarJehan et al., African J. Biotechnol., **10**(19), 3835 (2011).

[17] U.D. Altermatt, I.D. Brown, Ceramics Acta Crystallogr., **A43**, 121 (1987).

[18] C. G. Granqvist, Appl. Phys. A **57**, 19 (1993).

[19] Lung-Chien Chen, Chih-Ming Chen, Chie-Sheng Hong J.Electrochem.Soc, **153**, 931 (2006),

[20] N.Gul, T.Y Mujahid, S. Ahmed, Pak. J. Bio. Soc. **7**(1), 2055 (2004).

[21] O. Lupan, Th. Pauporte, V.V. Ursaki, I.M. Tiginyanu, Opt. Mater. **33**, 914 (2011).

[22] O.Yamamoto, M. Hotta , J. Sawai , T. Sasamoto , H. Kojima J. Ceram. Soc. Japan. **106**, 1007 (1998).